Estimating the Crustal Power Spectrum From Vector Magsat Data

David A.J. Lowe,[1] Robert L. Parker,[1] Michael E. Purucker[2] and Catherine G. Constable[1]

Short title: CRUSTAL POWER SPECTRUM

Submitted to J. Geophys. Res., April 2002.

[1]Cecil H. and Ida M. Green Institute of Geophysics and Planetary Physics, Scripps Institution of Oceanography, University of California at San Diego, La Jolla, CA.

[2]Geodynamics Branch and Raytheon ITSS, Goddard Space Flight Center, Greenbelt, MD.

Abstract. The Earth's magnetic field can be subdivided into core and crustal components and we seek to characterize the crustal part through its spatial power spectrum (R_l). We process vector Magsat data to isolate the crustal field and then invert power spectral densities of flight-local components along-track for R_l following *O'Brien et al.* [1999]. Our model (LPPC) is accurate up to approximately degree 45 (λ=900 km) - this is the resolution limit of our data and suggests that global crustal anomaly maps constructed from vector Magsat data should not contain features with wavelengths less than 900 km. We find continental power spectra to be greater than oceanic ones and attribute this to the relative thicknesses of continental and oceanic crust.

Introduction

Sabaka et al. [2000] have simultaneously modeled the internal and external parts of the near-Earth magnetic field using observatory and satellite data. This work allows us to isolate the crustal signal (vector summation of remanent and core-induced fields) in Magsat data. We seek to characterize the crustal field through its power spectrum (R_l) for a number of reasons. Firstly, by estimating R_l directly from the data, and not spatially modeling the crustal field before constructing it, we can guide the production of crustal anomaly maps. Specifically, it is possible to identify at what wavelengths the power in the anomaly maps diverges from our direct estimate and suggest the maximum spherical harmonic degree to which the maps should be expanded. Secondly, the crustal field can be treated as correlated noise in core field studies by introducing off-diagonal terms into the covariance matrix. *Rygaard-Hjalsted et al.* [1997] (based on the work of *Jackson* [1990, 1994]) expressed the covariance matrix as a function of R_l and showed that an accurate model of R_l allows the construction of more accurate core field models from data collection systems with low noise levels. The recently (February 1999) launched Ørsted satellite has the potential to provide such high quality data. However, Magsat operated at lower altitudes than Ørsted and may be better suited to estimating an R_l that could be used to compensate for the Earth's crust in satellite based studies.

The geomagnetic power spectrum is defined to be the mean squared value of the magnetic field's magnitude per degree l. We express R_l (at the surface of the Earth)

using the Schmidt semi-normalized Gauss coefficients (g_l^m, h_l^m) of the crustal magnetic potential:

$$R_l = (l+1)\sum_{m=0}^{l}(g_l^m)^2 + (h_l^m)^2 \tag{1}$$

In estimating R_l we follow the approach of *O'Brien et al.* [1999] (who expanded on the work of *Mcleod and Coleman* [1980]) that connects one dimensional along-track power spectral densities (PSDs) with R_l. *O'Brien et al.* [1999] estimated the PSDs of flight-local vector components along arcs of great circles or great circle paths (GCPs). *O'Brien et al.'s* equations are listed below, where P_{ab} are the power- (a=b) or cross-spectral densities of the parallel-to-track (x), perpendicular-to-track (y) and radial (z) directions estimated at a distance r from the center of the Earth, a is the radius of the earth (6371 km), l and m are spherical harmonic degree and order respectively, $P_l^m(cos\theta)$ are the semi-normalized associated Legendre functions and $D_l^m(cos\theta)$ are their derivatives with respect to θ (co-latitude):

$$P_{xx}(k)=4\pi a\sum_{l=|m|}^{\infty}\left(\frac{a}{r}\right)^{2l+4}\frac{m^2P_l^m(0)^2}{(l+1)(2l+1)}R_l \tag{2a}$$

$$P_{yy}(k)=4\pi a\sum_{l=|m|}^{\infty}\left(\frac{a}{r}\right)^{2l+4}\frac{D_l^m(0)^2}{(l+1)(2l+1)}R_l \tag{2b}$$

$$P_{zz}(k)=4\pi a\sum_{l=|m|}^{\infty}\left(\frac{a}{r}\right)^{2l+4}\frac{(l+1)P_l^m(0)^2}{2l+1}R_l \tag{2c}$$

$$P_{xz}(k)=4\pi a\sum_{l=|m|}^{\infty}\left(\frac{a}{r}\right)^{2l+4}\frac{imP_l^m(0)^2}{2l+1}R_l \tag{2d}$$

O'Brien et al. made a number of assumptions in deriving these linear relationships

which are implicitly carried over into this paper. The Earth's crustal magnetic field is represented as one realization of a stationary, stochastic process where the Gauss coefficients of the crustal magnetic potential are taken to be independent random variables with zero mean and variance dependent only on l. These statistics are assumed to be rotationally invariant which allows every GCP to be treated as equatorial ($\theta = \frac{\pi}{2}$) and results in the flight-local (x,y,z) components being equivalent to the standard (r,θ,ϕ) ones. The use of great circles implies a constant radius of observation and coupled with the rotational invariance means that the covariance between any components at any position is solely a function of angular separation of the observation points. It is evident from eqn. 2d that the P_{xz} cross-spectra is non-zero and purely imaginary and it follows that its phase should be $\frac{\pi}{2}$ and coherence should be high. We use these properties along with the power sum rule ($P_{xx} + P_{yy} = P_{zz}$) [*Parker and O'Brien,* 1997] to test the above assumptions.

The P_{ab} in equations 2a-d represent ensemble averages of the along-track power spectra. By ensemble we imagine an infinite number of planets resembling the Earth. It is obviously impossible to carry out this kind of sampling and instead we average over this Earth, acknowledging that over this smaller set, stationarity may not be strictly upheld. We treat individual Magsat passes as independent samplings and average their associated PSDs together. Vector measurements made along GCPs are rotated into parallel-to-track, perpendicular-to-track and radial directions (x,y,z) in order to estimate the power spectral densities (P_{xx}, P_{yy} and P_{zz}) and cross-spectra (P_{xz})

along-track. We directly invert for R_l from our estimates of P_{ab} following equations 2a-d. Treating the crustal field as a stochastic process may appear to be flawed from a more deterministic viewpoint as geological processes create structure in the crustal magnetic field (for example, stripes on the ocean floor, highs over volcanic complexes). However, these features typically have wavelengths below Magsat's sensitivity. We take a global perspective and characterize the crustal field spectrally at wavelengths relevant to satellite studies.

Data Selection and Processing

To isolate the crustal component in Magsat vector data we use the comprehensive model (CMP3) of *Sabaka et al.* [2000]. This detailed model is derived from observatory and satellite (Pogo and Magsat) data and accurately reproduces the known, systematic behavior of the near-Earth field between 1960 and 1985. CMP3 includes contributions from the core field (4253 parameters), the crust (4160 parameters), the ionosphere (5520 parameters), the magnetosphere (800 parameters) and F-region currents that couple between the ionosphere and magnetosphere and between hemispheres (2088 parameters). The core, ionosphere and magnetospheric fields are modeled as the gradient of spherical harmonic expansions. The core field is expanded to spherical harmonic degree 13 (2730 parameters) and its secular variation (1523 parameters) is parameterized using B-splines in time. The ionospheric and magnetospheric spherical expansion coefficients are dependent on solar fluxes and modulated by diurnal and seasonal frequencies. The

ionospheric coefficients are taken to be linear functionals of the solar flux index $F_{10.7}$ and the magnetospheric ring current is modeled to be proportional to the D_{st} index. As these external contributions vary with time they induce fields in the Earth and these are calculated under the assumption of a 4-layer radially varying conductivity model. The fields produced by coupling (field-aligned and meridional) currents flow within Magsat's shell of observation and consequently can not be modeled as gradients of potential functions. It is assumed that these currents are primarily radial and the associated fields are represented through separate toroidal stream functions that are also modulated by diurnal and seasonal frequencies.

The flowchart in Fig. 1 outlines our data processing and selection procedure. **Figure 1.** The original 1 Hz data, supplied on CD-rom by NASA-GSFC, is decimated to 0.1 Hz to reduce the size of the dataset which contains 5712 individual passes. No crustal information is lost because the data's Nyquist wavenumber lies far above the signal-noise transition of the crustal field. Following subtraction of CMP3's prediction for the core and external fields, we are left with the unmodeled components of the core and external fields in addition to the desired crustal signal. At the surface of the Earth, the crustal field has been shown to dominate the core field at wavelengths less than 2750 km and so we will restrict our study to shorter wavelengths to avoid contamination by large core field residuals. To minimize the presence of external signal individual passes are curtailed at $\pm 50^o$ dipole latitude and rejected if the solar K_p index rises above 1^+ because external field behavior becomes more complex at high geomagnetic latitudes

and during periods of high solar activity.

In another automated pre-processing step any passes with length less than 150 datapoints are rejected. This is designed to avoid large gaps in the series of observations that may lead to spurious structure when the vector data are interpolated and rotated from the supplied (N,E,V) system to the desired (x,y,z). Our spectral estimation scheme requires uniform along-track sampling and a spacing of 76 km is chosen because it corresponds to the original 0.1 Hz interval. The passes are then subdivided into descending (dawn) and ascending (dusk) limbs which facilitates the introduction of an important consistency check. If we have truly isolated the crustal signal, the power spectra derived from these subsets should be equivalent because the crustal field does not vary on short timescales. At this point 1955 'good' passes remain: 962 dawn and 993 dusk.

It is inevitable that non-crustal features will still exist at this pre-processed stage and individual visual inspection is carried out to search for spatially sharp tears and spikes that could not have originated in the Earth's crust. Specifically we highlight large amplitude, small scale structures that are uncorrelated with the scalar data (attitude related noise) or correlated with sustained high K_p values (unmodeled external contributions). In addition, the aforementioned spectral tests (power sum rule and P_{xz} cross-spectra) are performed. If a pass satisfies these constraints it is retained; in total, 260 dusk and 199 dawn passes are kept and used to estimate P_{xx}, P_{yy}, P_{zz} and P_{xz}

along-track. Our selection criteria reduce the dataset to 8% of its original size. This may seem extreme and raise suspicions that the subset of the data we have selected using the spectral tests is not representative and so would bias our estimate of R_l. Poor data quality is the most common reason for failure of the spectral tests and in order to investigate whether the spectral tests reject satisfactory data, we re-inspect the 'good' dawn dataset to highlight 149 passes whose vector component records look 'perfect' (some of the 'good' passes contain small tears or spikes that do not appear to influence the spectral tests). 101 (or 68%) of these 'perfect' passes possess the expected spectral characteristics. Furthermore, 34 of the 48 passes that do not satisfy both spectral tests, display the appropriate P_{xz} phase and coherence and fail the power sum rule test largely due to the behavior of P_{yy}, which will be discussed shortly. Thus, it does not appear that using the spectral tests to discard data is introducing bias into our results.

Our robust multitaper spectral estimation technique is based upon the sinusoidal tapers of *Riedel and Sidorenko* [1995]. The Nyquist for each P_{ab} is identical (common sampling interval), but owing to the slightly different pass lengths, the wavenumbers at which the spectrum is evaluated are not the same. To average the spectra, wavenumber bins are required and the size of 0.0001 cycles/km is chosen. This value is large enough to hold a significant number of datapoints yet small enough to retain detail and downplay bias. The averaged along-track PSDs are shown in Fig. 2.

Figure 2.

PSD Results

It is important to understand how closely our PSD estimates resemble the true PSDs and we investigate this through the use of noise-free synthetic data. The semi-normalized Gauss coefficients are represented as normally distributed random variables with zero mean and variance dependent only on l. The variance is then related to R_l:

$$\sigma_l^2 = \frac{R_l}{(l+1)(2l+1)} \tag{3}$$

We simulate many sets of Gauss coefficients from a single R_l and generate vector data along many GCPs at altitudes comparable to Magsat's. We estimate average PSDs from the simulations and compare them to those calculated directly from R_l using eqn. 2. It was found that the PSDs matched perfectly at wavelengths less than approximately 3000 km. This indicates the shortcomings of our sampling and spectral estimation techniques, PSDs at wavelengths longer than 3000 km cannot be accurately estimated from GCPs with typical lengths of 12000 km.

The theory of *O'Brien et al.* [1999] assumes that measurements are made on a great circle but Magsat's orbit had an apogee of 561 km and a perigee of 352 km. We investigate the significance of this departure from theory by generating synthetic vector data from equivalent dipole sources. Fig. 3 shows along-track spectral test results from orbits with a 450 km uniform altitude (approximate mean of Magsat)

Figure 3.

compared to ones with Magsat's specifications. It is not possible to directly compare the actual PSDs as the average altitudes of these particular orbits are not equal to 450 km; all circular PSDs are greater than the elliptical ones, reflecting the lower average observation altitude (approximately 415 km). First, we note that the circular orbit results agree with theoretical predictions at all wavenumbers up until the point where noise dominates signal. This suggests that if noise (non-crustal signal) is minimal the spectral tests are not hindered by the truncation of the passes. Second, the elliptical orbit results agree with the circular results and theoretical predictions in an intermediate wavenumber range (0.0005-0.0016 cycles/km). This demonstrates that in addition to difficulties in estimating P_{ab} at the longest wavelengths from GCPs, variation in altitude also introduces bias in this region. Consequently, we view our estimates at wavelengths greater than 3000 km with suspicion but note that this is not such a limiting factor in our analysis because residual core signal is a likely contaminant at wavelengths greater than 2750 km.

From Fig. 2 it can be seen that at the longest wavelengths the dawn and dusk power spectral densities (PSDs) do not agree within their error limits for any component and that the dusk spectra are greater than dawn. It should be noted that no correction has been made for the different average observation altitudes of these subsets (397 km for dusk and 426 km for dawn) but that this is not necessary because on a logarithmic scale the difference between PSDs synthesised at 397 and 426 km is imperceptible. We select the common signal from the independent dawn and dusk subsets by retaining

the wavenumbers below the signal-to-noise transition (indicated by change in slope of the spectrum and the shrinking of errorbars) at which the dawn and dusk estimates of P_{ab} agree within error limits (region denoted by broken lines in Fig. 2). The dawn and dusk estimates of P_{xz} do not agree and it is discarded. Fig. 4 shows the results of the spectral tests performed on the dawn and dusk subsets.

Figure 4.

The power sum rule is approximately upheld for both dawn and dusk subsets in an intermediate wavenumber region sandwiched between low wavenumber contamination and high wavenumber noise processes. The cross-spectral P_{xz} tests return better results, adhering to the theory more closely and over a broader wavenumber range. This suggests that the y-component is more contaminated than x or z because the power sum rule uses all three components whereas the P_{xz} tests use x and z only. Inspection of the individual spectra reveals that P_{yy} has the least overlap between dawn and dusk subsets and comparison of this overlap with the waveband of power sum rule agreement supports the hypothesis that the y-component is polluting the power sum rule test. On the basis of these results P_{yy} is also discarded.

The geometry of the GCPs is such that the y-component is most closely aligned with lines of constant latitude (ϕ-direction) and so an obvious potential source of contamination in P_{yy} are ionospheric currents that flow parallel to lines of constant longitude (in the θ-direction). These types of currents are often referred to as field-aligned currents because the Earth's core field is dominantly dipolar. At low-latitudes field-aligned

currents are associated with the equatorial electrojet, as suggested by [*Untiedt*, 1967] and discussed in detail by [*Langel et al.*, 1993]. At mid-latitudes, the inter-hemispheric current system suggested by *Van Sabben* [1966] has been identified in Magsat data by *Olsen* [1997]. Both of these currents systems are incorporated in CMP3 but it is possible that one or both were not perfectly modeled and residual currents exist in the dataset.

As discussed above, part of reason for the long wavelength disparity between dawn and dusk estimates of P_{ab} may be due to altitude effects and/or spectral estimation difficulties. However, the fact that dusk is uniformly significantly greater than dawn suggests that these biases are not wholly responsible. External contributions are greater at dusk compared to dawn and so we suspect the presence of unmodeled external signal and/or elevated externally induced fields. An estimate of the RMS magnitude of this 'extra' signal can be obtained by calculating the square root of the difference in integrated PSDs estimated at dusk and dawn local times. This value is 9.8 nT for P_{xx}, 13.8 nT for P_{yy} and 17.4 nT for P_{zz}, a signal of magnitude 24 nT. CMP3 uses a radially varying, spherically symmetric conductivity model of the Earth to calculate the field induced by time dependent components of the ionospheric and magnetospheric fields. Therefore, it is possible that this discrepancy is at least partly due to 3-dimensional induction effects. *Everett et al.* [1999] have shown that oceans, continents and shelves can account for as much as 50% of the total induced signal. If electromagnetic induction is a component of this disagreement, the dusk-dawn contrast between PSDs estimated over oceans, P^o_{ab}, compared to those estimated over continents, P^c_{ab}, will be greater.

This is because sea water is significantly more conductive than lithospheric rocks. Fig. 5 reveals that the mean P_{zz} contrast estimated over oceans is indeed considerably greater than that estimated over continents and similar behavior is observed with other components.

Figure 5.

A strict interpretation of the term 'stationary' implies that every GCP would produce an identical PSD for each component. Obviously this is not the case and in fact it would be somewhat disappointing if the Earth's crust could be modeled as a realization of a single stationary, stochastic process. Continental and oceanic crusts possess different chemical compositions, thicknesses and formation processes and so one would expect there to be a difference between P_{ab}^{c} and P_{ab}^{o} observed at the same local time. As was discussed above, the dusk oceanic passes appear to be contaminated by unmodeled induced fields and so we restrict our attention to the dawn subset. Fig. 6 depicts P_{ab}^{o} and P_{ab}^{c} for the x and z-components and it can be seen that the oceanic spectra contain less power than the continental ones.

Figure 6.

The explanation for this result probably lies in the fact that continental crust is thicker than oceanic. Oceanic crust is typically more highly magnetized than continental crust but there is a larger volume of continental crust and the product of thickness with magnetization appears to be greater for continents than for oceans. Other authors have noted the disparity between continental and oceanic crust from a magnetic standpoint; for example, *Hinze et al.* [1995] reduced magnetic anomalies

to vertical polarizations and found the mean radially polarized magnetic anomaly of the continents to be greater than that of the ocean at the 99.9% confidence level. A cursory inspection of crustal anomaly maps (e.g. *Ravat et al.* [1995]) reveals most of the high amplitude anomalies (e.g. Bangui, Kursk) lie on continents. These observations suggests an avenue for further work, separating the oceans from the continents in a statistical sense. It is important to realize that this result does not invalidate our model of R_l, only underscores it as one representative of 'this' Earth as a whole.

Having estimated P_{ab} we are in a position to estimate the resolution limit of the data. The wavenumber at which P_{xx} and P_{zz} decay to zero, where signal becomes masked by noise, can be considered to be this limit - approximately degree 45 or 900 km (Fig. 2). Thus, crustal anomaly maps constructed from this vector data should not contain features with wavelengths less than 900 km. It should be noted that this resolution limit value is representative of the Earth's crust as a whole and regional studies over high amplitude crustal anomalies may yield more detailed information. This value is in good agreement with the 920 km estimate of *Arkani-Hamed and Strangway* [1986]. *Sailor et al.* [1982] derived a resolution limit of 700 km for a number of passes over the eastern Indian Ocean based on the coherence of scalar data. In addition to the regional nature of this estimate, scalar data are attitude independent and insensitive to field-aligned currents and so a higher resolution limit is to be expected.

The Inverse Problem

We perform a joint linear inversion of P_{xx} and P_{zz} for R_l following the theory published in chapter 3 of *Parker* [1994]. An overview of the inverse problem is presented here and the reader is referred to *O'Brien et al.* [1999] for a more detailed description. Re-writing eqn. 2 highlights P_{ab} as a linear functional of R_l, where Q^l_{ab} is the weighting vector that relates R_l to P_{ab} at a specific wavenumber (k):

$$P_{ab}(k) = \sum_{l=1}^{\infty} Q^l_{ab} R_l \tag{4}$$

Fig. 7 shows Q^l_{xx} and Q^l_{zz} for k=0.00065 cycles/km or m=26 calculated at 410 km altitude (the average observation altitude of the dawn and dusk subsets). The sensitivity of R_l to a datapoint is greatest at the corresponding wavelength, diminishes with decreasing wavelength and is null to data at longer wavelengths. Thus, regularization can be used to control the model at wavelengths where there are no data (outside l=25-45). We invert for a model of R_l up to l=100 that is smooth (sum of second derivatives), small and fits the data within the ascribed errorbars; a minimizer of:

Figure 7.

$$U = \|\mathbf{Rm}\|_2^2 + \alpha\|\mathbf{m}\|_2^2 + \beta\left(T^2 - \|\mathbf{\Sigma}\left(\mathbf{d} - \mathbf{Wm}\right)\|_2^2\right) \tag{5}$$

where $\mathbf{m}$ is the sought model, $\mathbf{d}$ is the data (averaged dawn and dusk PSDs), $\mathbf{W}$ is the weights matrix whose rows are Q^l_{ab} for different datapoints, $\mathbf{R}$ is the second derivative matrix, T is the tolerance (the expected departure of model prediction from noisy data, *Parker* [1994]) and $\mathbf{\Sigma}$ is the inverse of the covariance matrix with $\frac{1}{\sigma_i}$ on the diagonal,

where σ_i is the error assigned to the datapoint d_i. There are two Lagrange multipliers involved; α (=600) is arbitrarily chosen to force the model to be of minimum size before and after the data controlled section (l=25-45) and β (=691) is adjusted until the misfit to the data is unity. A smooth model is simpler to explain physically and by including a size constraint we minimize unnecessary structure in the model. There are an infinite number of models that satisfy eqn. 5 and we reduce this degeneracy by selecting the positive one with the smallest 2-norm.

Results and Discussion

Our model (LPPC) is non-zero between degrees 5 and 70 forming a smooth asymmetric peak (30 nT^2) at degree 28 and is displayed in Fig. 8 in comparison to a selection of other non-regional estimates [*Cain et al.*, 1989; *Jackson*, 1994; *Ravat et al.*, 1995; *O'Brien et al.*, 1999 and *Sabaka et al.*, 2000]. The solid lines (LPPC and *O'Brien et al.* [1999]) in Fig. 8 represent models that have been constructed through regularized inversion. *O'Brien et al.* [1999] estimated along-track PSDs from a number of oceanic aeromagnetic vector passes collected during Project Magnet. The low observation altitude (7 km) facilitates accurate estimation of R_l up to degree 1200 but the relatively short track lengths (5000 km) hamper model development at degrees lower than 60. Thus LPPC and *O'Brien et al.'s* model are complementary and should not strictly be compared. It should also be noted that since *O'Brien et al.'s* model is based solely on oceanic data we would expect it to contain less power than

Figure 8.

our global model because we found P_{ab}^{o} to be significantly less than P_{ab}^{c} at dawn local time.

The individual symbols in Fig. 8 (*Cain et al.*, 1989, *Ravat et al.*, 1995 and *Sabaka et al.*, 2000) represent estimates that have been empirically constructed following eqn. 1 from sets of crustal Gauss coefficients. There is no requirement for these estimates to be smooth or otherwise well-behaved, they are by-products of spatial field modeling. The models of *Sabaka et al.* and *Cain et al.* include the core field and points below l=13 lie outside of Fig. 8 due to their large magnitude. *Sabaka et al.'s* estimate of R_l that is plotted in Fig. 8 is the weighted summation of the crustal Gauss coefficients (up to degree 65) that were solved for in the development of CMP3. We used CMP3 to remove contributions from the core, ionosphere and magnetosphere and further isolated the crustal field by visually inspecting and performing spectral tests on the data and through the comparison of average PSDs estimated from the independent dawn and dusk subsets. *Sabaka et al.* write that their estimate of R_l, and by association their spatial crustal model, is valid up to degree 43 (λ = 930 km) which is in accord with our suggested resolution limit for Magsat vector data. The estimates of *Cain et al.* and *Ravat et al.* are built solely from satellite data and their quality is dependent on the level of sophistication of their crustal isolation schemes. *Ravat et al.'s* treatment of external fields is superior to *Cain et al.'s* and this is reflected in the higher degree to which the estimates appear valid, degree 60 compared to degree 45. *Jackson's* [1994] k_3 is a theoretical estimate and is plotted as a broken line. *Jackson* modeled the lithosphere as a collection of random but spatially correlated distribution of magnetizations and

adjusted his model parameters to match *Cain et al.'s* [1989] empirical estimate from l=15-45 and to set the intergal of the model to 300 nT^2, the approximate RMS value of the lithospheric field based on observatory biases (e.g. *Bloxham et al.* [1989])

There is wide disagreement between these published estimates that is caused by a number of factors; different data, different crustal isolation schemes and different methods of constructing R_l (forward modeling, inversion and empirical estimation from Gauss coefficients). Consequently, it is impossible to say definitively which is the 'best'. However, it is possible to answer the question: do any of these models fit P_{xx} and P_{zz} in the wavenumber region where crustal signal dominates? It is straightforward to convert these models into pseudo-data through the weights matrix $\mathbf{W}$ and calculate the misfit ratio, M, using:

$$M = \frac{\|\Sigma\,(\mathbf{d} - \mathbf{W}\mathbf{m})\,\|}{T} \tag{6}$$

For comparison *Cain et al.'s* model is windowed to include l=16-45, *Sabaka et al.'s* model is windowed to include l=16-43, *Ravat et al.'s* is truncated at l=60 and the models of *O'Brien et al.* and *Jackson* include terms to higher degree than shown in Fig. 8, l=1200 and 1800 respectively. The fit of the various models to the estimates of P_{xx} and P_{zz} are shown pictorially in Fig. 9. Obviously LPPC has a M-misfit ratio of 1.0, but *Cain et al.*, *Sabaka et al.* and *Jackson* are respectable with ratios of 1.3, 1.4 and 1.8 respectively. It is unsurprising that *Cain et al.* and *Jackson* perform in a similar fashion

Figure 9.

as the latter was based on the former in a degree range (l=15-45) that is highly relevant to satellite studies. The models published by *Ravat et al.* ($M = 3.2$) and *O'Brien et al.* ($M = 2.9$) do not contain enough power. *O'Brien et al.* do not consider their model to be reliable below l=60 and as we have suggested, ocean-based models are biased low from a global standpoint, so this underprediction is expected. *Ravat et al.* go to great lengths in their attempts to minimize non-crustal signal, performing pass-by-pass correlations and covariant analysis on dawn and dusk anomaly maps. These procedures make for very robust anomaly maps but perhaps some crustal signal has inadvertently been removed in the process and this is evidenced by the underprediction of the model. It could also be argued that we have not been thorough enough and that in the wavenumber region where dusk and dawn estimates agree the PSDs are still inflated with non-crustal noise.

The strength of LPPC lies in the detailed separation of the crustal field using CMP3 and the flexible, non-automated approach taken in the key steps of data processing. It has been shown that the initial assumptions are reasonable by checking the spectral tests (power sum rule, P_{zz} coherence and phase) for each pre-processed pass and rejecting those that fail. It is difficult to obtain high degree estimates from satellite data because of the nature of upward continuation; the shortest wavelengths become attenuated and overlap with noise sources. LPPC is based on data collected at satellite altitude and as such does not return values for the total power in the crustal field at the Earth's surface comparable with observatory biases. LPPC characterizes the crustal field observed in vector Magsat data and can be used to guide construction of crustal anomaly maps and

remove the crustal magnetic signal from satellite data in order to accurately model the core field. To produce a more geologically relevant model a joint inversion of satellite and aeromagnetic vector data could be performed taking into account the differences observed between continental and oceanic power spectra.

Conclusion

In making a few simple assumptions about the nature of the crustal magnetic field we have produced a smooth model of the crustal power spectrum. The data have been carefully processed, tested, visually inspected and windowed to minimize the presence of non-crustal signal. Comparison of along-track PSDs for dawn and dusk subsets of the data reveals discrepancies at long wavelengths which represent approximately 24 nT of unmodeled signal at least partially caused by 3D induction effects and field-aligned currents. The windowed PSDs are inverted for a positive power spectrum that balances size, smoothness and misfit. LPPC compares satisfactorily with other satellite based models up to degree 45, where a lack of data hampers our efforts to estimate R_l accurately. Degree 45 (900 km wavelength) is then the resolution limit of our data and suggests that global crustal anomaly maps constructed from vector Magsat data should not contain features with wavelengths less than 900 km.

References

Arkani-Hamed, J. and D. W. Strangway, Band-limited global scalar magnetic anomaly map of the Earth derived from Magsat data, *J. Geophys. Res., 91* 8193-8203, 1986.

Bloxham, J.,D. Gubbins and A. Jackson, Geomagnetic secular variation, *Phil. Trans. R. Soc. Lond., 329* 415-502, 1989.

Cain, J. C., Z. Wang, C. Kluth and D. R. Schmidtz, Derivation of a geomagnetic model to n=63, *Geophysical Journal, 97*, 431-441, 1989.

Everett, M. E., S. Constable and C. G. Constable, Modeling and observing 3-D satellite geomagnetic induction, *EOS, 80*, F298, 1999.

Hinze, W. J., R. R. B. von Frese and D. N. Ravat, Mean magnetic contrasts between oceans and continents, *Tectonophysics, 192*, 117-127, 1989.

Jackson, A., Accounting for crustal magnetization in models of the core magnetic field, *Geophys. J. Int., 103*, 657-674, 1990.

Jackson, A., Statistical treatment of crustal magnetization, *Geophys. J. Int., 119*, 991-998, 1994.

Langel, R. A., M. Purucker and M. Rajaram, The equatorial electrojet and associated currents as seen in MAGSAT data, *J. Atmos. Terr. Phys., 55*, 1233-1269, 1993.

Mcleod, M. and P. J. Coleman, Spatial power spectra of the crustal geomagnetic field and core geomagnetic field, *Phys. Earth Planet. Inter., 23*, 5-19, 1980.

O'Brien, M. S., R. L. Parker and C. G. Constable, The magnetic power spectrum of the

ocean crust on large scales, *J. Geophys. Res., 104*, 29189-29201, 1999.

Olsen, N., Ionospheric F region currents at middle and low latitudes estimated from Magsat data, *J. Geophys. Res., 102*, 4563-4576, 1997.

Parker, R. L., *Geophysical Inverse Theory*, 386 pp., Princeton, New Jersey, 1994.

Parker, R. L., and M. S. O'Brien, Spectral analysis of vector magnetic field profiles, *J. Geophys. Res., 102*, 24815-24824, 1997.

Ravat, D., R. A. Langel, M. Purucker, J. Arkani-Hamed and D. E. Alsdorf, Global vector and scalar Magsat magnetic anomaly maps, *J. Geophys. Res., 100*, 20111-20120, 1995.

Riedel, K. S., and A. Sidorenko, Minimum bias multiple taper estimation, *IEEE Trans. Sig. Proc., 43*, 188-195, 1995.

Rygaard-Hjalsted, C., C. G. Constable and R. L. Parker, The influence of correlated crustal noise in modeling the main geomagnetic field, *Geophys. J. Int., 130*, 717-726, 1997.

Sabaka, T. J., N. Olsen and R. A. Langel, A comprehensive model of the near Earth magnetic field : Phase 3, NASA/TM-2000-209894, 75 pp., 2000.

Sailor, R. V., A. R. Lazarewicz and R.F. Brammer, Spatial resolution and repeatability of Magsat crustal anomaly data over the Indian ocean, *Geophys. Res. Lett., 9*, 289-292, 1982.

Untiedt, J., A model of the equatorial electrojet involving meridional currents, *J. Geophys. Res., 72*, 5799-5810, 1967.

Van Sabben, D., Magnetospheric currents associated with the N-S asymmetry of Sq, *J.*

Atmos. Terr. Phys., *28*, 28965-28981, 1966.

C. G. Constable, Cecil H. and Ida M. Green Institute of Geophysics and Planetary Physics, Scripps Institution of Oceanography, University of California at San Diego, 9500 Gilman Drive, La Jolla, CA 92093-0225. (e-mail: rlparker@ucsd.edu)

Received _____

This manuscript was prepared with AGU's LaTeX macros v5, with the extension package 'AGU++' by P. W. Daly, version 1.6b from 1999/08/19.

Figures

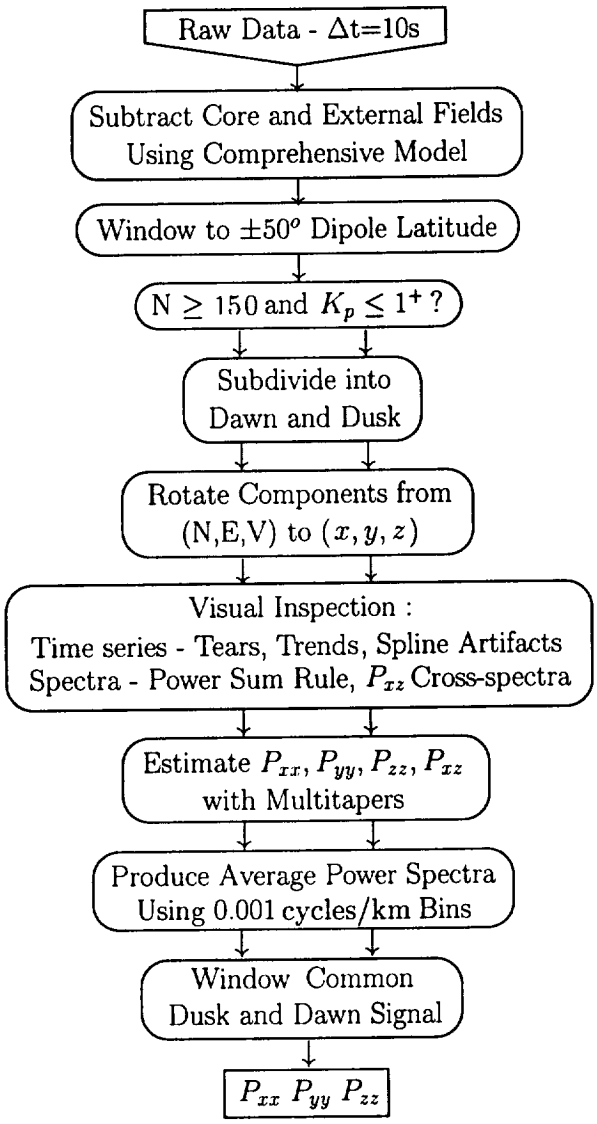

Figure 1. Flow chart displaying the various steps taken in processing and selecting the data.

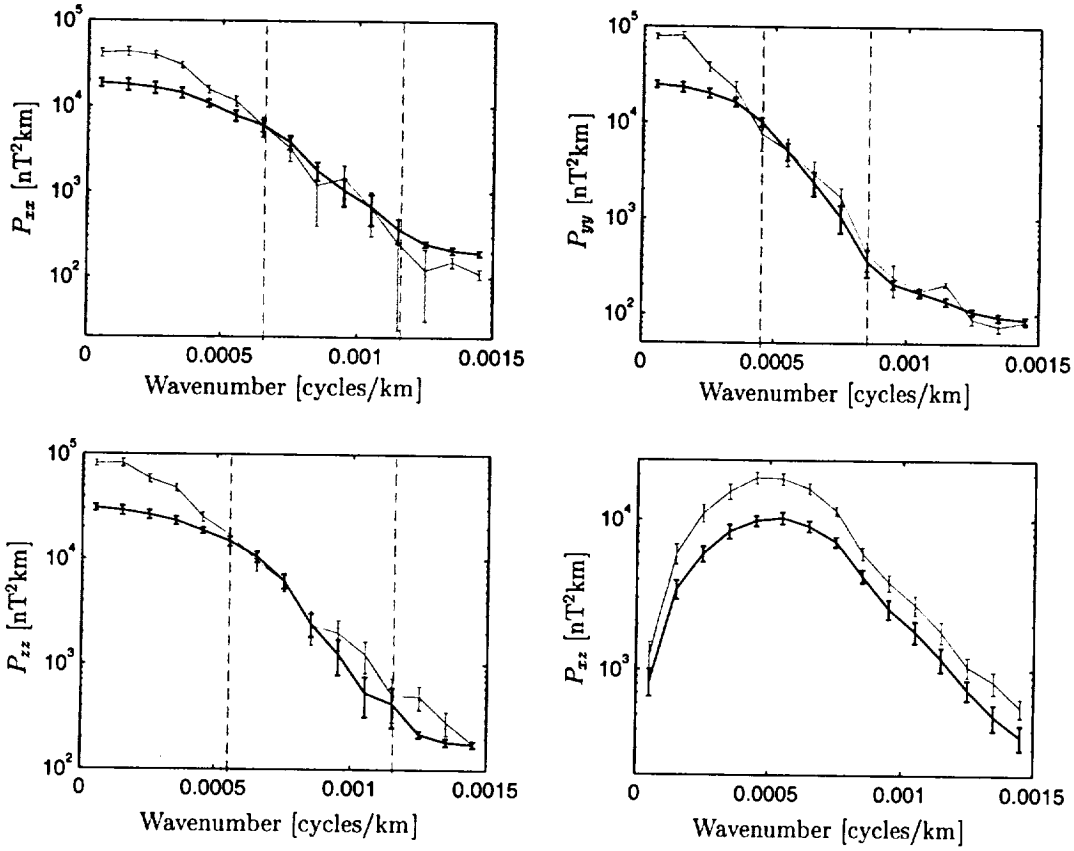

Figure 2. Averaged along-track power spectra (P_{xx}, P_{yy}, P_{zz}, P_{xz}) for dawn (dark) and dusk (light) subsets of the processed data. The errorbars represent two standard error in the mean of the subsets (95% confidence). The spectra are windowed to include the wavenumbers at which the dawn and dusk estimates agree within the error limits above the noise floor (indicated by broken vertical lines). The dawn and dusk estimates of P_{xz} do not overlap and this data is discarded. The dusk estimate of each spectrum is greater than the dawn estimate at long wavelengths which suggests the presence of unmodeled external features and/or elevated induced fields in the data as external fields are greater in magnitude at dusk than dawn.

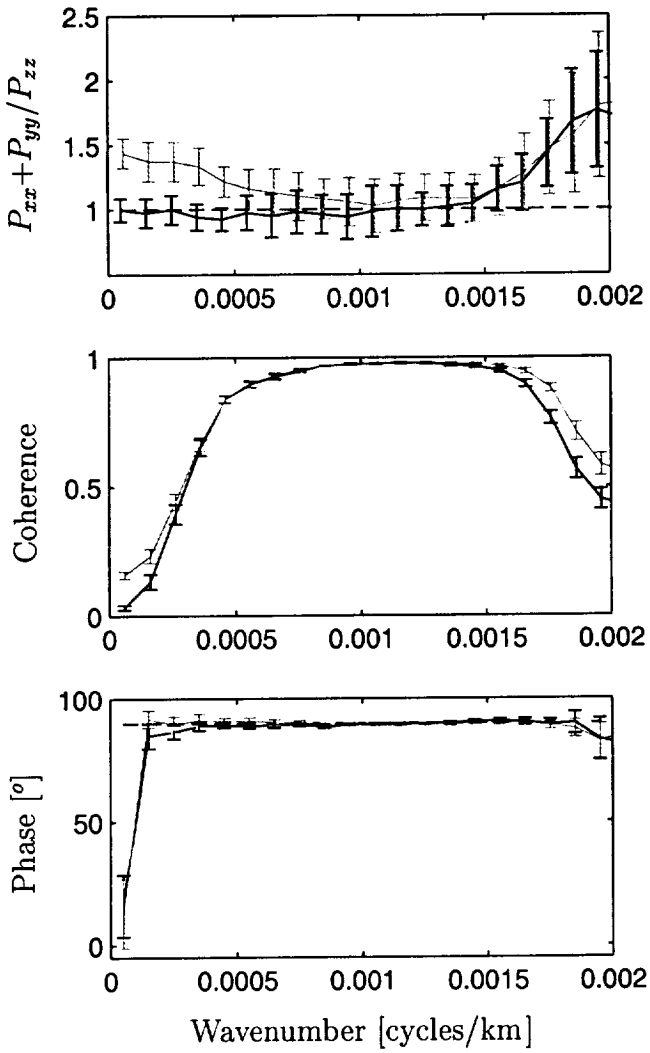

Figure 3. Along-track power spectral tests performed on orbits whose radius varies like Magsat (light) and those of uniform radius (dark) as required in *O'Brien et al.'s* [1999] theoretical development. The errorbars represent two standard error in the mean (95% confidence) and the broken lines indicate theoretical predictions. Values from both orbits diverge from theoretical predictions at wavenumbers greater than 0.0015 cycles/km which indicates the dominance of noise. At long wavelengths the circular orbit values agree with theory but elliptical results do not. This suggests that a varying observation altitude distorts spectral results at wavelengths longer than 2000 km. Thus, the theory can be applied in an intermediate wavenumber range, 0.0005-0.0015

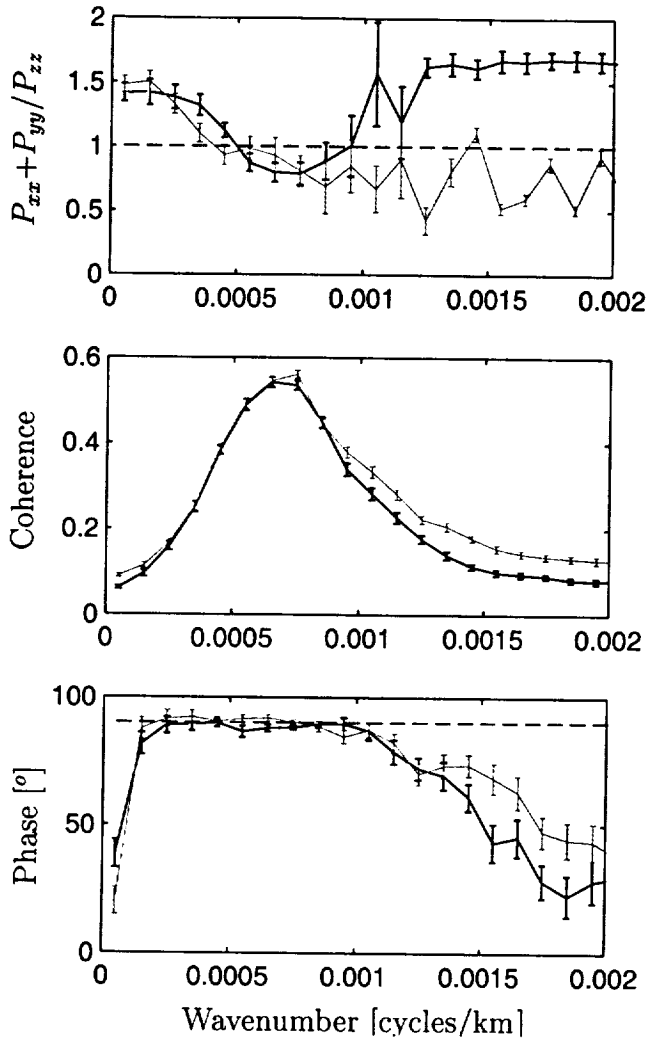

Figure 4. Along-track power spectral tests performed on dawn (dark) and dusk (light) subsets of the processed data. The broken lines indicate theoretical predictions and the errorbars represent two standard error in the mean of the subsets (95% confidence). The power sum rule is obeyed most closely for both dawn and dusk subsets in a narrow wavenumber band (0.0005-0.0008 cycles/km) contrasting to the broader adherence of the P_{xz} tests (0.0003-0.001 cycles/km). This indicates that the y-component is of lesser quality than the x and z components as the power sum rule reflects the behavior of all three components and the P_{xz} tests only use the x and z components. Comparison of the waveband of power sum rule agreement with the overlap of dusk and dawn estimates of P_{yy} in Fig. 3 confirms that the y-component is contaminating the power sum rule test.

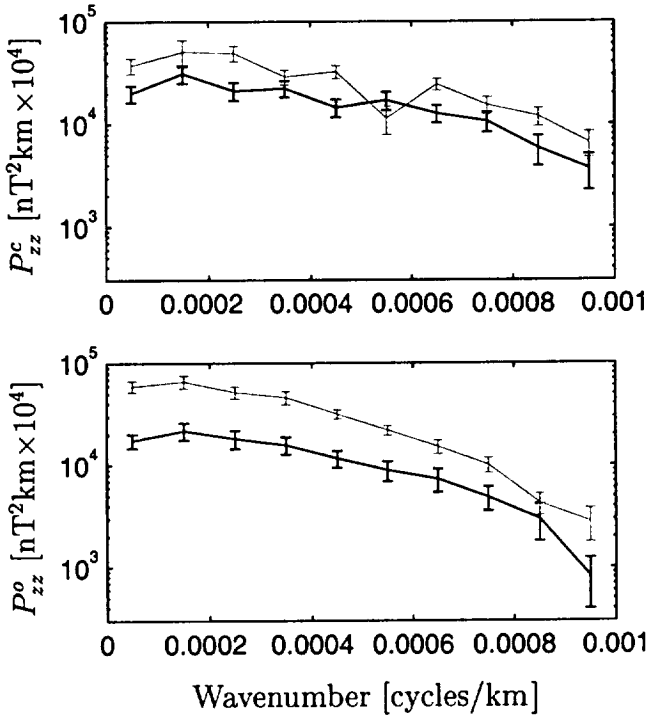

Figure 5. P_{zz} along-track power spectra for dawn (dark) and dusk (light) estimated over oceanic and continental lithosphere. The errorbars represent two standard error in the mean of the subsets (95% confidence). The greater difference between dusk and dawn subsets over the oceans compared to that over continents suggests that unmodeled induced fields are present in the crustal signal we have attempted to isolate.

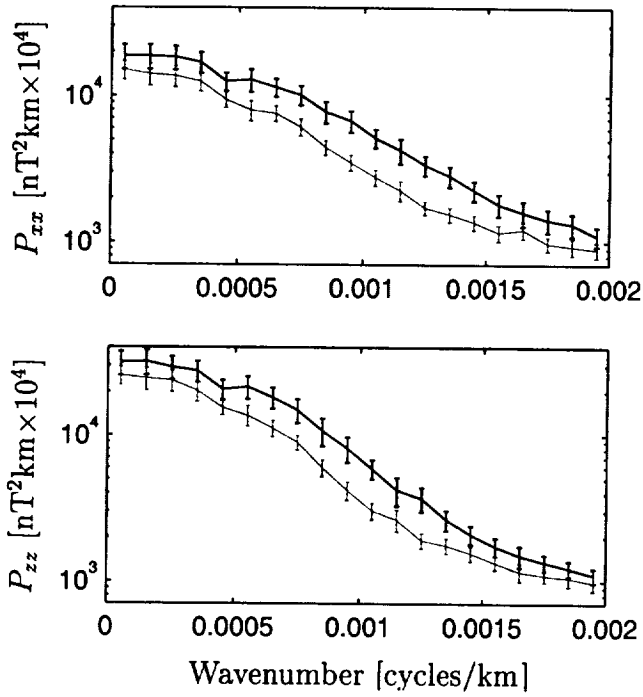

Figure 6. Dawn estimates of P_{xx} and P_{zz} along-track power spectra for oceanic (light) and continental (dark) lithosphere. The errorbars represent two standard error in the mean of the subsets (95% confidence). The continental spectra are greater than the oceanic at all wavenumbers and this relationship is most distinct in the intermediate wavenumber range 0.0005-0.0015 cycles/km.

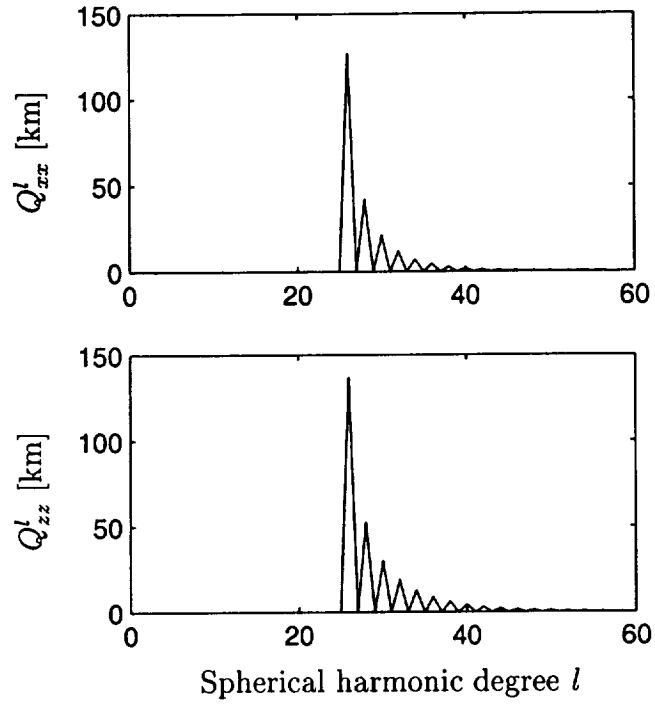

Figure 7. The weight functions that relate R_l to P_{xx} and P_{zz} show that the sensitivity of R_l to a datapoint is greatest at the corresponding wavelength, decreases with increasing wavelength and is null to data at longer wavelengths. The associated datapoint is m=26 or k=0.00065 cycles/km and the weights function is evaluated at 410 km altitude.

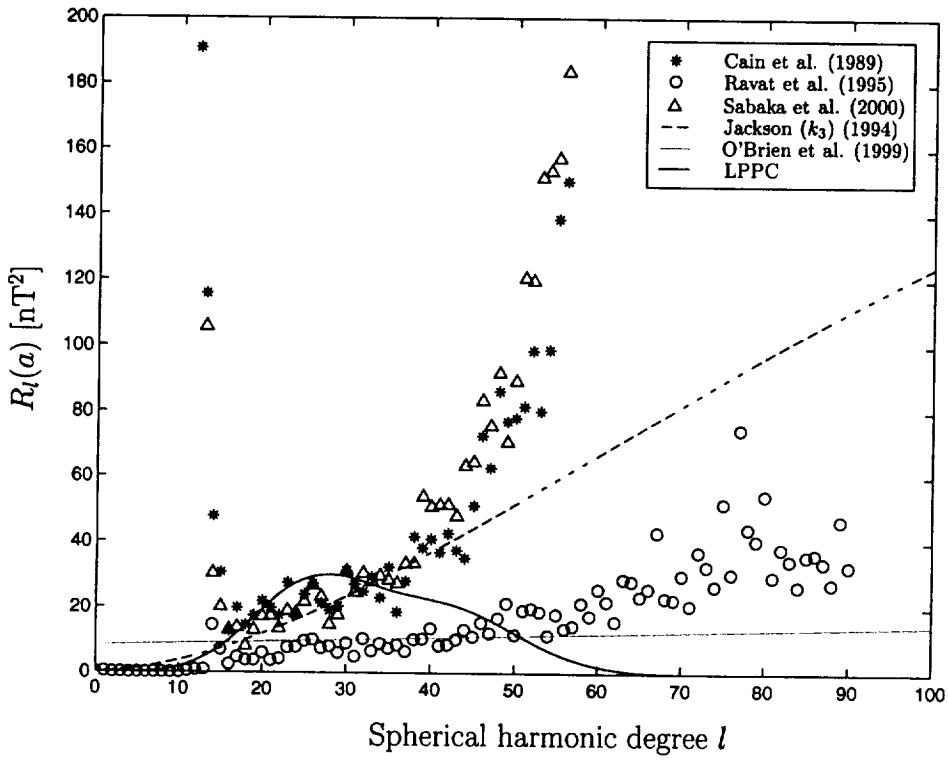

Figure 8. Comparison of published models of R_l at the Earth's surface - *Cain et al.* [1989], *Ravat et al.* [1995], *Sabaka et al.* [2000], *Jackson* [1994], *O'Brien et al.* [1999] and LPPC.

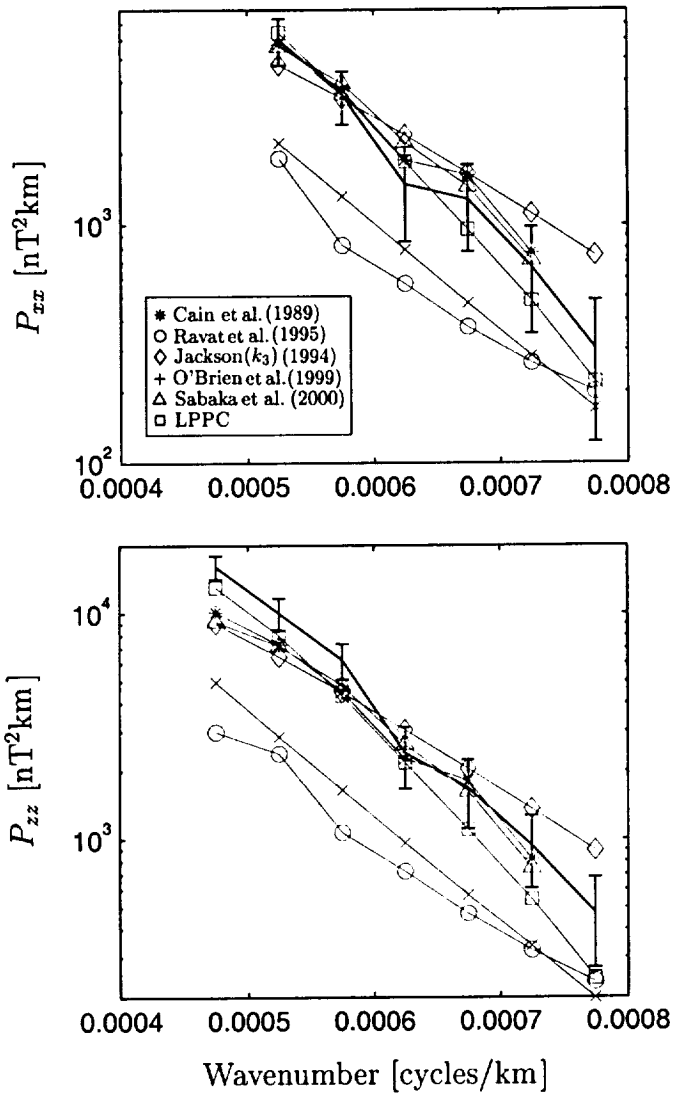

Figure 9. The models shown in Fig. 8 are converted into pseudo-data (light) through use of the weight functions and compared to actual data (dark). LPPC is show to fit the best, followed by *Cain et al.* [1989], *Sabaka et al.* [2000], *Jackson* [1994], *O'Brien et al.* [1999] and *Ravat et al.* [1995].